JOURNAL OF BIOMEDICAL OPTICS 3(2), 145–153 (APRIL 1998)

IMAGING AND QUANTITATION OF A TISSUE-SELECTIVE LANTHANIDE CHELATE USING AN ENDOSCOPIC FLUOROMETER

Michael P. Houlne,[†] Darren S. Hubbard,[†] Gary E. Kiefer,[‡] and Darryl J. Bornhop[†]
[†]Texas Tech University, Department of Chemistry and Biochemistry, Lubbock, Texas 79409-1061;
[‡]Dow Chemical Company, Designed Chemicals R&D, Freeport, Texas 77541

(Paper JBO-132 received Jan. 7, 1997; revised manuscript received Sep. 26, 1997; accepted for publication Oct. 10, 1997.)

ABSTRACT

Tissue spectroscopy and endoscopy are combined with a tissue site-selective fluorescent probe molecule to demonstrate *in vitro*, spatial, remote, quantitative imaging of the rat small intestine. The probe molecule employed, Tb-3,6,9-tris(methylene phosphonic acid *n*-butyl ester)-3,6,9,15-tetraaza-bicyclo[9.3.1]pentadeca-1(15),11,13-triene (Tb–PCTMB), is shown to bind with the small intestine and provide improved image contrast. High sensitivity is possible due to the absorption-emission Stokes's shift exhibited by the Tb–PTCMB complex. Excitation is centered near 270 nm and multifeatured emission is observed at 490, 550, 590, and 625 nm. Sprague-Dawley rats were dosed with the Tb-PTCMB complex, which shows biodistribution, leading to preferential binding to the inner surface of the small intestine. It is shown that the fluorescent image, taken at 550 nm, can be used to quantify the amount of Tb–PCTMB present in an excised tissue sample. The 3σ detection limits are found to be in the femtomole range. An optical mass balance for Tb–PCTMB-dosed small intestine is performed and along with radiotracer biodistribution, demonstrates that approximately 40% of the marker probe resides in the endothelial tissue of the small intestine inner lumen. This result is of particular interest since most adult colon cancers develop in this region. These results demonstrate the ability to perform spatial, quantitative, *in vitro*, endoscopic imaging of a complex biological sample using a probe marker. © *1998 Society of Photo-Optical Instrumentation Engineers.* [S1083-3668(98)00302-5]

Keywords lanthanide chelate; endoscopic imaging; tissue selectivity; fluorescence.

1 INTRODUCTION

Significant advances have been made in the area of tissue spectral analysis and it now appears possible to both identify and grade a tumor with the use of these approaches.[1–6] Currently, work has been directed toward contrasting native spectroscopic signals of normal and abnormal tissue in an effort to generate spectrochemical fingerprints useful for tissue diagnosis.[2,3,5] However, to effectively treat tumors, they must be identified and histopathologically graded in early stages of development. Such detection can be problematic since small tissue abnormalities often yield only low spectrochemical signatures or relatively small spectral changes. It can be difficult to measure the contrast of these small signals since surrounding normal tissues often exhibit large background spectral signals.

Effective clinical identification and evaluation of abnormal tissue at the earliest stages of development is best accomplished remotely and with minimal invasion.[7–12] In addition, such analysis should be multidimensional in nature. That is, it should provide quantitative, spectroscopic information about the tissue itself as well as spatial information (tissue surface area). Steps toward multidimensional imaging using endoscopy have been demonstrated in several areas of tissue evaluation. These include histopathological investigation of human artery wall tissue using Raman spectroscopy,[3] fluorescence detection of abnormal cervical tissue,[13] detection of dysplasia or carcinoma in the lung,[9] identification of colonic mucosa abnormalities,[14,15] and tracking of photodynamic cancer therapy.[16] In work by Mosher and co-workers,[16] a fluorescence microscope was used to construct a three-dimensional graph of fluorescence intensities found in OAT 75 cells loaded with the chlorophyll-derived photosensitizer, pheophorbide *a*. Digitizing the TV images of the samples allowed image reconstruction.

Cothren et al. have combined colonoscopy with laser-based spectroscopy to probe native fluorescence to optically grade ''observable'' abnormal tissues in the colon.[6] These results are quite promising, yet the technique is limited to either later-stage tissues or large sites. Lam et al. demonstrated that endoscopy can be combined with laser-excited autofluorescence to improve tissue spectra using a fluorescence bronchoscope imaging system based

Address all correspondence to Darryl J. Bornhop. Tel: (806) 742-3142; Fax: (806) 742-1289; E-mail: djbornhop@ttu.edu; Dr. Bornhop is also with the Southwest Cancer Center at the University Medical Center.

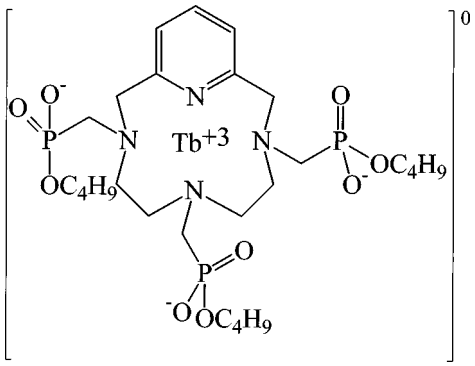

Fig. 1 Chemical structure for Tb-3,6,9-tris(methylene phosphonic acid *n*-butyl ester)-3,6,9,15-tetraaza-bicyclo[9.3.1] pentadeca-1(15), 11,13-triene, Tb–PTCMB.

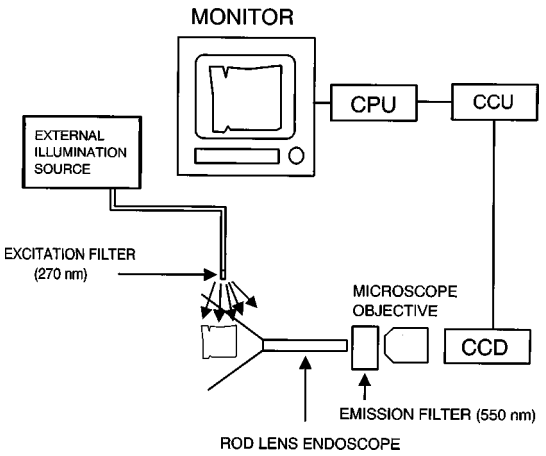

Fig. 2 Block diagram of the endoscopic fluorometer: CPU, computer; CCU, camera control unit; and CCD, black and white CCD camera. The microscope objective is a 5× lens.

on an He:Cd laser.[9] The detection of dysplasia and carcinoma of the lung is 50% better with spectroscopy than with white-light endoscopy.

One alternative approach to probing native spectroscopic properties is to employ a contrast enhancement agent, an exogenous molecular probe. Such techniques have been used in magnetic resonance imaging (MRI),[12,17–21] in the analysis of cellular function,[12,22] for the determination of localized pH in tissues,[23,24] for improved cancer detection,[25,26] and in the study of membrane potential and ion transport.[27–29] In particular, organic–metal chelate compounds have recently been shown to be useful as tissue site-selective markers.[17–21,24,30–33] However, some limitations in using chelates as probes have been low water solubility, poor molecular stability, and poor tunability of tissue site selectivity.

In contrast to the rare-earth fluorescent markers used earlier in analytical cytology,[33,34] we are using a new class of fluorescent probe molecules[28,35] with good chemical stability,[36] reasonable water solubility, and significant tissue site selectivity.[30–32] The probes are polyazamacrocyclic chelates of terbium. These markers are advantageous for tissue imaging for several reasons. First, because the chemical structure and molecular charge can be easily modified (by side-chain substitution), high tissue site selectivity is possible. In this paper it is shown that the PCTMB chelate is largely selective for the endothelial layer of the small intestine. Second, we have found that millimolar aqueous solutions exhibit no measurable cytotoxicity.[37] Third, they exhibit a large absorption-emission Stokes's shift,[30–32] improving contrast in biological matrix imaging by spectrally resolving the sample signature from the background fluorescence of the unaffected tissue.

In our present work we demonstrate spatial, quantitative, multidimensional, endoscopic imaging of rat small intestine *in vitro* using Tb-3,6,9-tris(methylene phosphonic acid *n*-butyl ester)-3,6,9, 15-tetraaza-bicyclo[9.3.1]pentadeca-1(15), 11,13-triene, or Tb–PCTMB (Figure 1). Our current optical train allows spatial imaging on the micron level and sensitivity to Tb–PCTMB at the subpicomole level.

2 EXPERIMENTAL

A block diagram of the endoscopic fluorometer is shown in Figure 2. The sample was affixed to a microscope slide, positioned using micrometer-driven translation stages, and illuminated with the light source. White light illumination was delivered by a fiber optic-coupled 150-W Xe microscope illuminator (Ziess, Germany). Fluorescence was initiated by a 75-W ultraviolet (UV) curing lamp (Dymax, Inc., Model PC-3) through a liquid light guide (Dymax, Inc.) coupled to a 270-nm interference filter with a 20-nm bandwidth (Omega Optical, part 270 BP20). As specified by the U.S. Food and Drug Administration (FDA), which states that ''biologically effective radiation cannot exceed 0.003 J/cm^2 for UV radiation between 180 nm and 400 nm,'' we determined that for a 5-s exposure time there was approximately 0.004 J/cm^2. This value is slightly higher than needed to negate carcinogenicity testing, but certainly close enough to the FDA limits to suggest clinical applicability. Fluorescent images were collected at about 90 deg to excitation with a 210-mm-long Hopkins plastic rod-lens endoscope (Model 1005-9029, Galileo, Inc.). The image from the scope was passed through a 550-nm interference filter with a 10-nm bandwidth (Omega Optical, part 550 DF10), magnified with a 5× glass microscope objective lens (further eliminating unwanted UV light by the collection optics), and directed onto a thermoelectrically cooled CCD (Model ST-6, Santa Barbara Instrument Group). The black-and-white CCD signal was displayed on a personal computer, frames were grabbed with the accompanying control software for the camera, and images were analyzed using Adobe Photoshop, Version 2.5. The images were analyzed as 8-bit im-

ages throughout the study. The specific performance of this optical system is described elsewhere;[31] however, a wide field of view (415 mm^2) with a limiting resolution of 181 line-pairs for millimeter (lp/mm) has been produced.

The blank or background noise for the measurement was established using undosed tissue and tissuelike substrates; the latter was a highly reflective, fibrous, solid matrix that has a morphology similar to that of the tissue studied. No signal was detected from any undosed sample using an integration time of 5 or 10 s, allowing for elimination of background subtraction methodologies. Control data on the ratios of light to dark banks were indistinguishable from one another and had a near-zero intensity value. The substrate standards were prepared on analytical-grade filter paper disks (Baxter, Model F215-75) 5 mm in diameter. Five samples were placed in the optical train and the fluorescence image was captured after a 5-s integration time. Using image processing software (Adobe Photoshop), the background fluorescence from the blanks was quantified by determining the fluorescence signal integrated over the imaged surface of the sample. The standard deviation (σ) for these blanks was calculated using the average fluorescence signal for each of the blank samples. These values were then used in the established way to determine the detection limit at the 3σ level.

The instrument was calibrated by infusing a known quantity of Tb–PCTMB into five disks. The calibration standards and the tissue sample were mounted in the same position relative to the scope. Aqueous solutions of Tb–PCTMB were prepared at concentrations of $1.4\times10^{-5}M$, $2.8\times10^{-5}M$, $5.5\times10^{-5}M$, and $1.1\times10^{-4}M$. Five microliters of a different Tb–PCTMB concentration were applied to each disk. Once dry, these disks had 0.07, 0.14, 0.275, and 0.55 nmol of Tb–PCTMB, respectively, infused within. The standard disks were placed in the sample holder and excited with 270-nm light. All samples were interrogated for fluorescence at a 5-s integration time. As shown in Figure 3, graphing the fluorescence signal from each of the disks (in gray scale) against the number of moles of Tb–PCTMB produces a linear calibration plot. This plot has been corrected for losses due to fluence (as discussed later). Furthermore, we used our fluence calculations to correct the gray-scale values for the tissue samples.

Tissue samples containing the site marker (lanthanide chelate) were obtained from Sprague-Dawley rats (180 to 220 g) injected with a 100-μl solution of the Tb–PCTMB complex (pH=7.5, $6\times10^{-6}M$) in the tail vein. The injected quantity of compound was roughly equivalent to 0.1 mg Tb–PCTMB/kg rat body weight. After 30 min, the animal was euthanized and the small intestine segment was removed. Several samples of small intestine from each of two rats were imaged. The

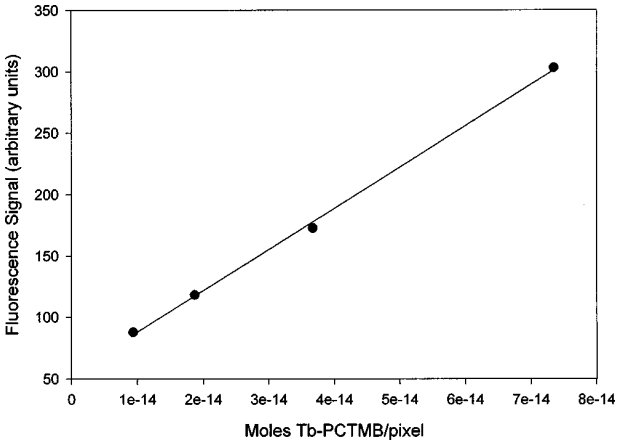

Fig. 3 Fluorescence signal versus concentration calibration plot, corrected for fluence losses.

samples weighed 3 mg each and were mounted in the sample holder with mounting wax. The fluorescent images were quantified and the amount of Tb–PCTMB was determined based on the calibration plot. The data presented are representative of the level of fluorescence detected within the ileum region of the organ. In addition to the fluorescence image, an image of the intestine sample was collected using a 150 W white light source for illumination with the emission filter removed.

In vivo biodistribution studies of the complex were also carried out using Sprague-Dawley rats. In this case, the same organic chelate was employed, except that the radioactive ^{153}Sm metal was used in the complex. A stock $^{153}SmCl_3$ solution was prepared by adding 2 ml of $3\times10^{-4}M$ of $^{153}SmCl_3$ (radioactive) in 0.1 N HCl to 2 ml of $3\times10^{-4}M$ $^{153}SmCl_3$ carrier solution. Appropriate ligand solutions were then prepared in deionized water. After the two solutions were thoroughly mixed (pH =2), the pH of the solution was raised to 7 using 0.1 N NaOH to facilitate complexation. Complexation was then evaluated by passing the sample solution (100 ml) through a Sephadex C-25 column, eluting (2×3 ml) with 4:1 saline (0.85% $NaCl/NH_4OH$), and comparing the amount of radioactivity in the eluent with that remaining on the column (free metal remains on the column). As earlier, Sprague-Dawley rats injected with the lanthanide chelate complex were euthanized after 30 min and their organs were removed. Radioactive counts from the tissue yielded the quantity of chelate in each of the tissue types.

3 RESULTS AND DISCUSSION

A qualitative white light image of the small intestine is shown in Figure 4(a). The view is of the inside of the lumen in a section of small intestine taken from the region known as the lower ileum. During dissection and mounting of the tissue sample, some of the mucosa layer pulled away

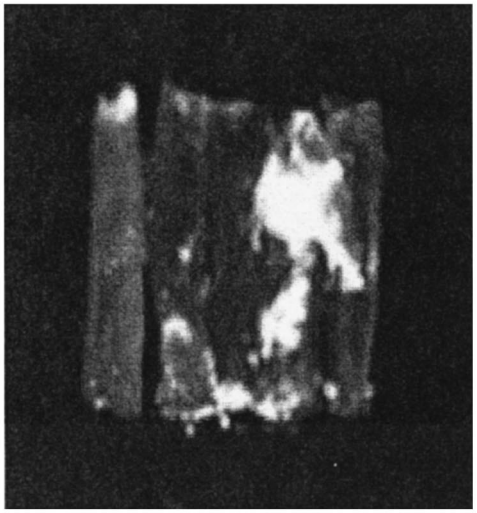

(a)

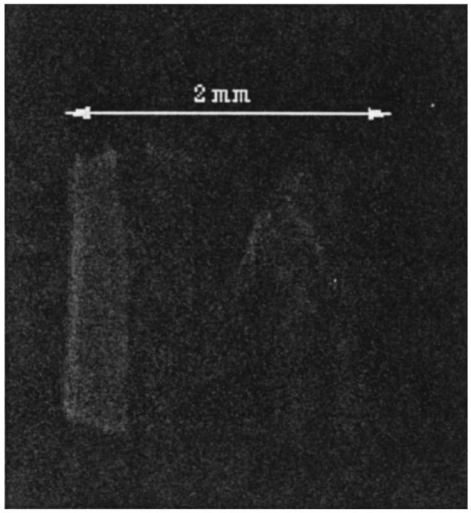

(b)

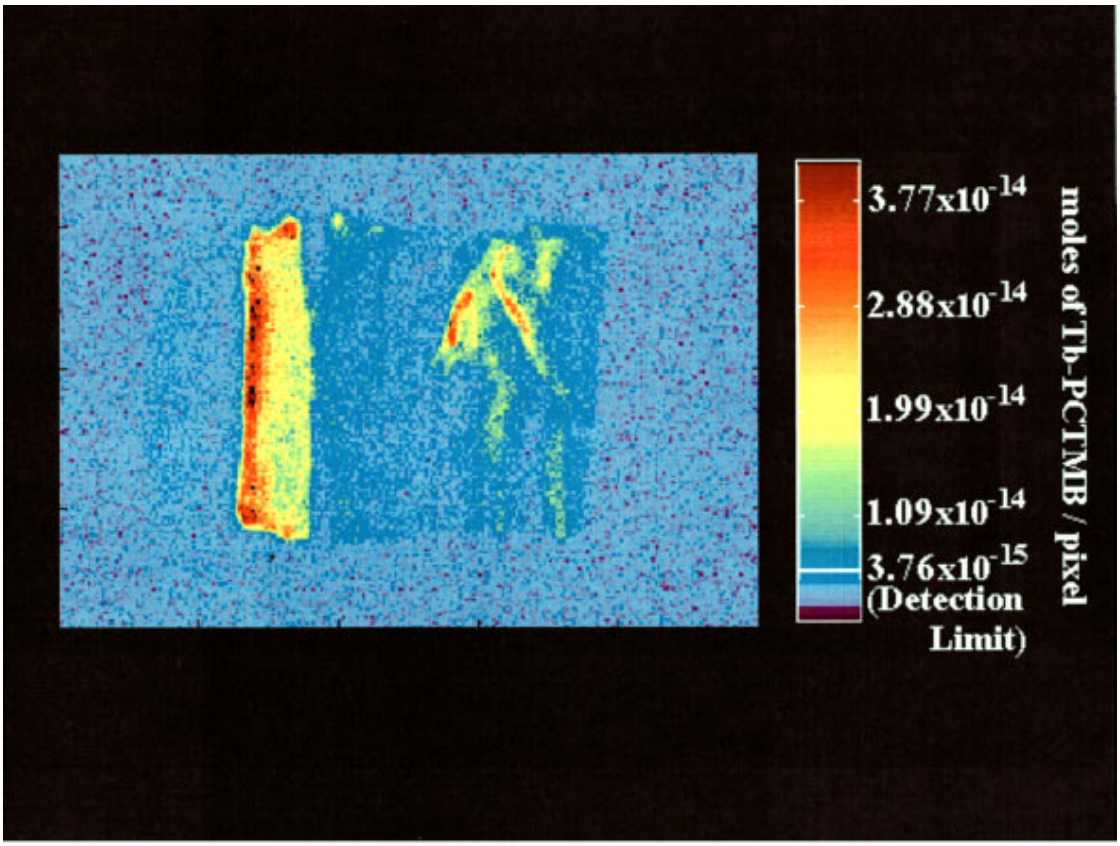

(c)

Fig. 4 (a) A diffuse reflectance white light image of the rat small intestine sample as collected by the endoscope. (b) Fluorescence endoscopic image of the sample. The rat was previously infused with 0.1 mmol/kg body weight of Tb–PCTMB. (c) A false color recreation of the fluorescence image showing preferential uptake and quantitation of solute.

from the surface lumen (e.g., the inside and edge of the lumen are shown in the unfolded tissue sample). This was inadvertent and was not necessary to generate the fluorescence signal. The left edge of the image shows a pseudoside view of a lumen wall and the connected mucosal lining. Tb–PCTMB appears to concentrate near the inner surface of the intestinal lumen (authors' unpublished results) and thus the high signal intensity found in the fluorescence image. Further studies are under way to understand the nonuniform distribution properties, uptake mechanism, and ''time-dependent'' penetration properties of the marker compound.

It should be noted that under the relatively low magnification used (with reference to the scale bar in the image), a fairly large viewing area is detected. Using a relatively low magnification and a wide field of view, at the expense of losing cellular detail, we were able to sample large regions in relatively short periods, which would be needed in clinical endoscopy. While the diffuse reflectance image provides little information about the morphology of the tissue, particularly solute uptake, the corresponding fluorescence image [Figure 4(b)] shows preferential uptake of the chelate into the inner lumen surface (the thick left edge of the tissue) and epithelial lining (the flap lying on top of the specimen that was torn during dissection). To further enhance the visualization of the site-specific binding observed in fluorescence detection, we constructed a false color contour plot [Figure 4(c)], which shows that uptake is not only preferential to the organ (small intestine), but also to a particular region of the intestine. Quantitation is needed to better understand this unique tissue site-binding mechanism, which allows utilization of the Tb–PTCMB chelates as biological makers. We have begun these investigations as reported here, using endoscopic fluorometry.

3.1 EXOGENOUS MARKER QUANTIZATION AND SYSTEM CALIBRATION

For quantitation of exogenous markers in actual tissue samples, there must be high confidence that the fluorescence signal emanates from the Tb–chelate and is representative of the fluorescent marker uptaken. In this study, no fluorescence was observed in dosed rat tissues other than the small intestine. Furthermore, virtually no fluorescence is observed if the chelate complex is not intact, because the unbound metal ion has a very low fluorescence cross section at 270 nm and when unbound metal ion is excited, the fluorescence is efficiently quenched by water molecules.[38] Although free Tb^{3+} has been used in transmission emission microscopy (TEM), it is not likely that free Tb ion from the complex is available to bind to DNA, owing to the large stability constants of the metal–chelate compounds. At the level of detection for the system (picomoles), an unexpectedly large emission quantum yield for a DNA–Tb^{3+} complex would be needed to produce an appreciable signal. Investigations of free metal ion–tissue equilibration are under way to ensure that this unlikely (because of complex stability and free ion toxicity) contributor to background does not interfere with the measurement. In addition, to perform these quantitative investigations, the sensitivity to photon flux must be determined. This calibration requires the determination of background signal (noise) and fluorescent signal as a function of analyte (signal intensity vs. moles).

As described in the experimental section, the standard deviation of background (noise) was evaluated using undosed substrates. Next a calibration plot for signal versus analyte quantity was constructed (Figure 3). Substrate disks were infused with a constant volume of increasingly concentrated Tb–PCTMB solution and allowed to dry. The disks were then imaged to determine the average fluorescence signal. A 7500-pixel area of the CCD was interrogated (the region with appreciable fluorescent signal), giving an intensity vs. position histogram that subsequently yielded the signal vs. concentration value. As shown in Figure 3, using a fixed integration time of 5 s, the response was found to be linear over 1.5 decades in concentration, with a correlation coefficient of $R=0.999$ and a slope of 3.36×10^{15} signal counts/mole.

The analytical sensitivity of any instrument can be defined by the minimal detectable quantity or detection limit. We calculate this limit at the 3σ level for an integration time of 5 s, where σ is the standard deviation of the mean fluorescence signal collected from five blank measurements. The blank measurements were made as described in the experimental section. Using the slope of the calibration plot and the relationship that $DL=3\sigma/\text{slope}$, the minimal detectable quantity was determined to be 3.73×10^{-15} mol Tb–PCTMB/pixel. The most concentrated standard (0.55 nmol) had a corrected fluorescence signal of 303. Above this concentration, the camera automatic antiblooming compensation circuitry produces gray scale value (GSV) levels that do not scale linearly with concentration. Adequate sensitivity is available at the modest integration times employed. Throughout the investigations we chose to use the most conservative estimate of detection limits to evaluate system performance, e.g., using σ under the worst-case scenario of short integration times.

The approximate detection limit per smallest imaging unit, the CCD pixel, is determined using a calibration plot of average fluorescence signal per pixel vs. moles of analyte per pixel. Rearranging the equation for the calibration plot yields $y=mx+b$, and the following result is obtained:

$$Q_{\text{avg.}}=2.98\times10^{-16}I-1.62^{-14} \quad (1)$$

where $Q_{\text{avg.}}$ is the moles of analyte per pixel and I is

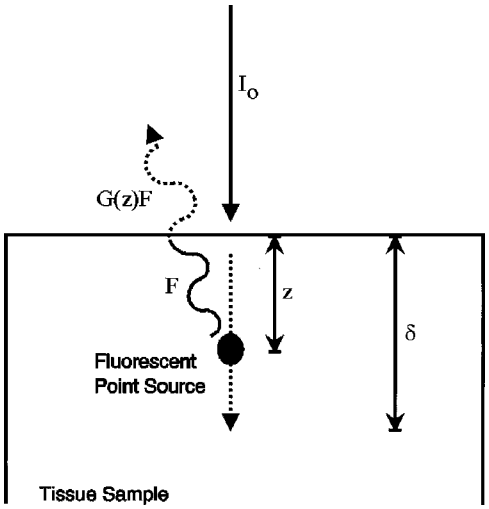

Fig. 5 A schematic diagram of an excitation source, I_0, penetrating a tissue sample to a depth δ. A fluorophore located a distance z below the surface emits a photon of intensity F. The escape intensity is $G(z)F$, where $G(z)$ is the escape function.

the fluorescence signal per pixel. Equation (1) is a direct relationship between average signal per pixel and quantity of analyte per pixel. With the use of Eq. (1), the total quantity of analyte in a sample region of any size may be estimated by multiplying $Q_{\text{avg.}}$ by the total number of pixels in the sampled image. Figure 4(c) shows the results of these calculations, allowing one to estimate the quantity of Tb–PCTMB in a particular region of the imaged tissue sample using the color scale.

To better quantify tissue-bound solute, we chose to determine the fluence rate and the escape function for the system to allow correction for excitation penetration depth and the amount of fluorescence that escapes from the medium using a model formulated by Gardner, Jacques, and Welch.[39] The method uses a Monte Carlo simulation that treats fluence rate and escape function with respect to the exponential attenuation of light from the source[39,40] and accounts for the dependency of light transport through the air-tissue surface boundary. Although a detailed discussion may be found elsewhere,[38] Figure 5 illustrates the assumptions employed in the present model. The tissue sample is considered homogeneous and large with respect to the penetration depth δ of the excitation source. The sample has an absorption coefficient, scattering coefficient, and scattering anisotropy denoted as μ_a, μ_s, and g, respectively. This is a one-dimensional model, assuming the excitation light is uniformly delivered normal to the surface and wide with respect to penetration depth. This assumes that the light distribution varies only with penetration depth. The fluence rate (ϕ) and escape function (G) are given, respectively, as follows:

$$\phi(z) = E_0[C_1 \exp(-k_1 z/\delta) - C_2 \exp(-k_2 z/\delta)] \tag{2}$$

$$G(z) = C_3 \exp(-k_3 z/\delta), \tag{3}$$

where z is the depth of the source fluorophore and C_1, C_2, C_3, k_1, k_2, and k_3 are parameters dependent on the diffuse reflectance, R_d. Empirical expressions for these seven parameters are given in Table 1.

Employing this one-dimensional light transport model, escape values dominate since the penetration depth of the excitation source (270 nm) is superficial (approximately 6 μm). Since the sample is studied *in vitro*, an air–tissue interface is present ($\eta_{\text{tissue}}/\eta_{\text{air}} = 1.38$) and the empirical equations in Table 1 may be used. Good approximations for μ_a and μ_s are 0.4 and 8 cm^{-1}, respectively, at 550 nm.[40] The empirical constants used to calculate $G(z)$ are

Table 1 Parameters for escape function calculations.

Parameter	$\eta_{\text{tissue}}/\eta_{\text{air}} = 1.38$	Calculated value
R_d	$\exp(-7\delta\mu_a)$	0.42
C_1	$3.09 + 5.44R_d - 2.12\exp(-21.5R_d)$	5.37
k_1	$1 - [1 - 1/\sqrt{(3)}]\exp(-20.1R_d)$	1.00
C_2	$2.09 - 1.47R_d - 2.12\exp(-21.5R_d)$	1.47
k_2	$1.63\exp(3.40R_d)$	6.80
C_3	$0.28 + 0.78R_d - 0.14\exp(-10.7R_d)$	0.61
k_3	$1 - 0.31\exp(-6.12R_d)$	0.98

Table 2 Results of quantitative calculations of Tb-PCTMB infused in the rat small intestine sample.

Sampled region	Fluorescence signal/pixel[a]	No. of sampled pixels	Total moles of Tb–PCTMB/pixel	Total moles of Tb–PCTMB[a]
1	130	1976	2.25×10^{-14}	4.44×10^{-11}
2	117	228	1.86×10^{-14}	5.37×10^{-12}
3	103	684	1.45×10^{-14}	9.91×10^{-12}

[a] Correlated for losses as dictated by fluence calculations.

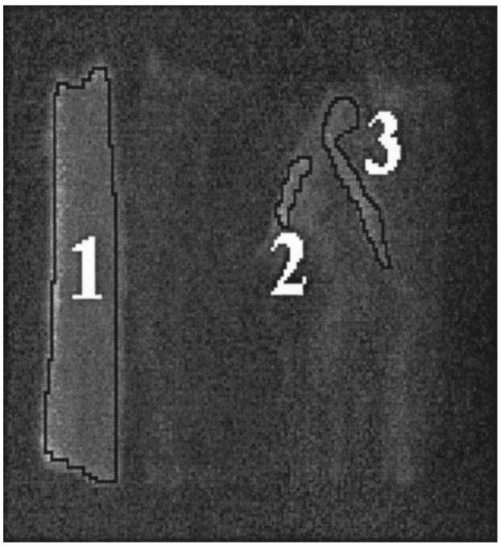

Fig. 6 Fluorescence endoscopic image of a 3-mg sample of rat small intestine showing the regions integrated for the mass balance calculations. The rat was previously infused with 0.1 mmol/kg body weight of Tb–PCTMB.

Table 3 Biodistribution results for radioactive Sm-PCTMB administered to Sprague-Dawley rats.

Tissue or organ	Percent distributed
Bone	3.73
Liver	2.70
Kidney	0.43
Spleen	0.05
Muscle	1.09
Blood	0.14
Heart	0.02
Lung	0.04
Brain	0.00
Stomach	0.08
Small intestine	57.98
Large intestine	0.77

given in Table 1. $G(z)$ is found to be 0.66 for a penetration depth of 6 μm, so only 66% of the fluorescence escapes from the tissue matrix. The corrected quantities of Tb–PCTMB in each of the three regions of the sampled tissue are given in Table 2. This escape correction was also applied to the standard substrate fluorescence signal used to generate Figure 3 and Eq. (1).

As a first approximation toward total solute quantitation, the small intestine fluorescence image may be divided in three parts, labeled 1, 2, and 3 and shown in Figure 6. These regions are chosen since their gray-scale values exceed that of the background. The quantity of Tb-PCTMB per pixel in each of these regions is found by first correcting the gray-scale values for fluence and then by using Eq. (1), derived from Figure 3. Next, the total quantity of Tb–PCTMB in each of the three regions is found by multiplying the average quantity of TB–PCTMB by the integrated sample area. Finally, the total quantity of marker in the small intestine sample, as determined by optical interrogation, is the sum of the three sampled regions. This sum corresponds to about 59.7 pmol. The results of these calculations are summarized in Table 2.

These results demonstrate our ability to quantify the presence of a probe marker in a complex biological matrix at the picomole level. While the current detection limits are quite low, considering the simplicity of the optical system and complexity of the sampled matrix, lifetime detection would likely further improve sensitivity and is possible because the chelates exhibit long-lived emission properties. This avenue is currently under investigation in our laboratories. However, even the smallest amount of solute found in sampled region 3 is 9.91 pmol, roughly a factor of 4 higher than the minimum detectable limit for an imaged region of this size (2.55 pmol).

3.2 MASS BALANCE COMPARISON

Next we set out to compare our optical quantitation results with results obtained using radioactive biodistribution (Table 3). It should be noted that the values for radioactivity in Table 3 do not add up to 100% because a portion of the chelate is passed through the excretory system. In the current study, each rat was dosed with 100 μl of a $1\times10^{-4}M$ Tb–PCTMB solution, which corresponds to a total injected dose of 1×10^{-8} mol of complex. From the biodistribution studies, we would expect that approximately 58% of the injected compound would be found in the small intestine. Therefore, our optical interrogation method should quantify a total of 5.80×10^{-9} mol in the entire length of the organ. Hence, a 3-mg sample of small intestine from a total mass of 120 mg, dosed and analyzed by either the radiotracer technique or fluorescence method, should contain about 145 pmol of solute. Here we randomly selected sample sections (3 mg) from the intestine of an animal dosed with 10 nmol of the Tb complex. Upon interrogation of this section of small intestine with our fluorescence endoscope, we obtained the fluorescence images shown in Figures 5(c) and 6 and calculated that the section contained about 59 pmol of solute (Table 2). This fluence-normalized value is only about a factor of 2.5 smaller than that predicted by nuclear chemistry and corresponds nicely to the expected value of 145 pmol. Of course if the total emission were used,

including the energy at wavelengths other than 550 nm, the quantity detected by the optical interrogation method would be more accurate.

It can be postulated that the difference between the expected solute quantity and the amount detected by fluorescence can be attributed to (1) the relatively short or limited penetration depth (6 μm) of the optical technique, allowing communication with just one or two epithelial cell layers; (2) the fact that the normal rat intestine epithelium is six to eight cells thick; and (3) the possibility of some of solute being bound in other parts of the small intestine. In the final analogy, the correlation between the two quantitation techniques is quite good, particularly given the small amounts of analyte administered or present in the tissue, the complexity of the matrix it lies within, and the simplicity of the instrumentation. Furthermore, the combination of quantitative endoscopic fluorometry for enhanced surface visualization with the recent observations suggesting selectivity of the Tb–PTCMB marker for colon tumors,[37] could expand the utility of colon endoscopy, since over 90% of adult small intestine cancers begin as inner lumen surface abnormalities.

While it has not been substantiated by experiment results, we believe that the pharmokinetics of Tb–PTCMB will be similar to that observed with compounds of similar structure, such as the Gd complex used for MRI contrast enhancement or the PDT photosensitizer aminoevulnic acid (ALA). In short, we expect that pathological tissues, such as tumors, will retain the complex much longer than normal epithelium.

4 CONCLUSION

We have demonstrated remote, spatial, quantitative, endoscopic imaging of biological tissues *in vitro*. This is possible using an effective injected dose of just 10 nmol. Through the use of tissue site-selective fluorescent markers, we have been able to detect picomole quantities of analyte in a region of the small intestine where an abnormality is most likely to develop. *In vivo*, femtomolar detection limits under minimally invasive imaging, as described, facilitate contrast enhancement to improve endoscopic visualization. Furthermore, the technique should allow solute analysis in biological research areas, including detection of local pH and investigation of ion transport mechanisms. Preferential uptake of the lanthanide chelate molecules by pathological tissue could allow for early warning, disease identification, or diagnosis in real time using endoscopic imaging, an opportunity being investigated in the laboratory and the clinic.

Acknowledgment

This research was funded by grants from the Texas Tech University (TTU) Research Enhancement Fund, the TTU Institute for Biotechnology, and the Whitaker Foundation. Special thanks to Galileo instruments for the donation of the rod lens endoscopes.

REFERENCES

1. S. Andersson-Engels, J. Johansson, S. Svanberg, and K. Svanberg, ''Fluorescence diagnosis and photochemical treatment of diseased tissue using lasers: Part II,'' *Anal. Chem.* **62**(1), 19A–27A (1990).
2. R. R. Alfano, C. H. Lui, W. L. Sha, H. R. Zhu, D. L. Akins, J. Cleary, R. Prudente, and E. Cellemer, ''Human breast tissue studied by IR Fourier transform Raman spectroscopy,'' *Lasers Life Sci.* **4**(1), 23–28 (1991).
3. R. Manoharan, J. J. Baraga, M. S. Feld, and R. P. Rava, ''Quantitative histochemical analysis of human artery using Raman spectroscopy,'' *J. Photochem. Photobiol. B: Biol.* **16**, 211–233 (1992).
4. K. Konig, H. Schneckenbuger, J. Hemmer, B. Tromberg, and R. Steiner, ''*In vivo* fluorescence detection and imaging of porphyrin-producing bacteria in the human skin and in the oral cavity for diagnosis of acne vulgaris, caries and squamous cell carcinoma,'' *Proc. SPIE* **2135**, 129–138 (1994).
5. Joint Symposium on Advanced Optical Techniques for Medical Diagnosis: Spectroscopy 1 & 2, Optical Society of America annual meeting and the 10th Interdisciplinary Laser Science Conference, October 1994; An International Symposium on Biomedical Optics, February 1995.
6. R. M. Cothren, R. Richards-Kortum, M. V. Sivak, M. Fitzmaurice, R. P. Rava, G. A. Boyce, M. Doxtader, R. Blackman, T. B. Ivanc, G. B. Hayes, M. S. Feld, and R. E. Petras, ''Gastrointestinal tissue diagnosis by laser-induced fluorescence spectroscopy at endoscopy,'' *Gastrointest. Endoscop.* **36**, 105–111 (1990).
7. P. Rol, R. Jenny, D. Beck, F. Frankahauser, and P. F. Niederer, ''Optical properties of miniaturized endoscopes for ophthalmic use,'' *Opt. Eng.* **34**, 2070–2077 (1995).
8. S. R. Goldstein, R. F. Bonner, R. L. Dedrick, F. H. Grantham, P. M. Gullino, C. C. Gibson, and D. A. McGuire, ''Fiber optic microfluoremetry for acute and chronic *in-vivo* animal studies,'' *J. Biomechanical Eng.* **102**, 265–273 (1980).
9. S. Lam, C. MacAulay, J. Hung, J. LeRiche, A. E. Profio, and B. Palcic, ''Detection of dysplasia and carcinoma *in situ* with a lung imaging fluorescence endoscope device,'' *J. Thoracic Cardiovasc. Surg.* **105**, 1035–1040 (1993).
10. C. C. Hoyt, R. R. Richards-Kortum, B. Costello, B. A. Sacks, C. Kittrel, N. B. Ratliff, J. R. Kramer, and M. S. Feld, ''Remote biomedical spectroscopic imaging of human artery wall,'' *Lasers Surg. Med.* **8**, 1–9 (1988).
11. D. L. Wise and L. B. Wingrad, Jr. (eds.), Various chapters and related references in *Biosensors with Fiber-optics*, Humana Press, Clifton, NJ (1991).
12. R. P. Haugland and A. Minta, ''Design and application of indicator dyes,'' in *Noninvasive Techniques in Cell Biology*, B. H. Satir, ed., Chaps. 1 and 2, Wiley-Liss, New York (1990).
13. N. Ramanujam, A. Mahadevan, M. Follen-Mitchell, S. Thomsen, E. Silva, and R. Richards-Kortum, ''Fluorescence spectroscopy of the cervix,'' *Clin. Consul. Obgyn.* **6**(1), 62–66 (1994).
14. R. Richards-Kortum, R. P. Rava, R. E. Petras, M. Fitzmaurice, M. Sivak, and M. S. Feld, ''Spectroscopic diagnosis of colonic dysplasia,'' *Photochem. Photobiol.* **53**, 777–786 (1991).
15. D. M. Melville, J. R. Jass, B. Morson, D. J. Pollock, P. I. Richman, N. A. Shepherd, J. K. Ritchie, S. B. Love, and J. E. Lennard-Jones, ''Observer study of the grading of dysplasia in ulcerative colitis: comparison with clinical outcome,'' *Human Pathology* **20**, 1008 (1989).
16. G. Moser, A. Ruck, H.-J. Schwarzmaier, and C. Westphal-Frosch, ''Photodynamic cancer therapy: fluorescence localization and light absorption spectra of chlorophyll-derived photosensitizers inside cancer cells,'' *Opt. Eng.* **31**, 1441–1446 (1991).
17. C. F. G. C. Geraldes, A. D. Sherry, I. Lazar, A. Miseta, P. Bogner, E. Berenyi, B. Sumegi, G. E. Kiefer, K. McMillan, F. Maton, and R. N. Muller, ''Relaxometry, animal biodistribution, and magnetic resonance imaging studies of some new

gadolinium (III) macrocyclic phosphinate and phosphonate monoester complexes,'' *Magnetic Res. Med.* **30**, 696–703 (1993).
18. G. K. Kiefer, J. Simon, and J. R. Garlich, ''Biocycloazamacrocyclophosphonic acids, their complexes and conjugates for use as contrast agents and processes for their preparation,'' World Patent WO94/26754 (1994).
19. A. D. Sherry and G. E. Kiefer, ''Alkyl phosphonate polyazamacrocyclic chelates for MRI,'' U.S. Patent 5,362,476 (1994).
20. W. D. Kim, D. C. Hrncir, G. E. Kiefer, and A. D. Sherry, ''Synthesis, crystal structure and potentiometry of pyridine-containing tetraazamacrocyclic ligands with acetate pendant arms,'' *Inorg. Chem.* **34**, 2225–2232 (1995).
21. S. Aime, M. Botta, and M. Sisti, ''MRI contrast agents: macrocyclic lanthanide (III) complexes with improved relaxation efficiency,'' *J. Chem. Soc. Chem. Commun.* **18**, 1885–1886 (1995).
22. S. Phimphivong, S. Kolchens, P. L. Edmiston, and S. S. Saavedra, ''Time-resolved, total internal reflection fluorescence microscopy of cultured cells using a Tb chelate label,'' *Anal. Chem. Acta.* **307**, 403–417 (1995).
23. R. K. Jain and G. R. Martin, ''Noninvasive measurement of interstitial pH profiles in normal and neoplastic tissue using fluorescence ratio imaging microscopy,'' *Cancer Res.* **54**, 5670 (1994).
24. J. Devoisselle, V. Maunoury, S. Mordon, and D. Coustaut, ''Measurement of *in vivo* tumorous/normal tissue pH by localized spectroscopy using a fluorescent marker,'' *Opt. Eng.* **32**(2), 239–243 (1993).
25. S. Andersson-Engels, R. Berg, and S. Svanberg, ''Multicolour fluorescence imaging in connection with photodynamic therapy of delta-amino levulinic acid (ALA) sensitized to skin malignancies,'' *Bioimaging* **3**, 134–141 (1995).
26. M. Kriegmair, R. Baumgartner, and A. Hofstetter, ''Detection of early bladder cancer by 5-aminolevulinic acid-induced porphyrin fluorescence,'' *J. Urology* **155**, 105–110 (1996).
27. J. E. Gonzalez and R. Y. Tsien, ''Voltage sensing by fluorescence resonance energy transfer in single cells,'' *Biophys. J.* **69**, 1272–1280 (1995).
28. L. D. Taylor, S. R. Adams, and R. Y. Tsien, ''Special topic: quantitative microscopy. Controlling cell chemistry with caged compounds,'' *Ann. Rev. Physiol.* **55**, 755 (1993).
29. N. G. Publicover, E. M. Hammond, and K. M. Sanders, ''Amplification of nitric oxide signaling by interstitial cells isolated from canine colon,'' *Proc. Natl. Acad. Sci. U.S.A.* **90**, 2087–2091 (1993).
30. M. P. Houlne, G. F. Kiefer, and D. J. Bornhop, ''Spectroscopy characterization and tissue imaging using site-selective polyazacyclic terbium (III) chelates,'' *Appl. Spectrosc.* **10**, 225–244 (1996).
31. G. E. Kiefer and D. J. Bornhop, ''Fluorescent chelates as visual tissue-specific imaging agents,'' World Patent filed Oct. 11 (1996).
32. D. S. Hubbard, M. P. Houlne, G. E. Kiefer, H. F. Ianssen, C. Hacker, and D. J. Bornhop, ''Diagnostic imaging using rare-earth chelates,'' *Lasers. Med. Sci.,* in press (1998).
33. J. Simon, J. R. Garlick, D. A. Wilson, and K. McMillan, ''Bone marrow suppressing agents,'' U.S. Patents 4,882,142 and 4,976,950, issued 1989 and 1990.
34. R. C. Leif and L. M. Vallarino, ''Rare-earth chelates as fluorescent markers in cell separation and analysis,'' ACS Symposium Series Vol. 464, *Cell Separation Science and Technology*, D. S. Kompala and P. W. Todd, eds., pp. 41–58, American Chemical Society, Washington, DC (1991).
35. W. D. Kim, G. E. Kiefer, F. Maton, K. McMillan, R. N. Muller, and A. D. Sherry, ''Relaxometry, luminescence measurements, electrophoresis and animal biodistribution of lanthanide (III) complexes of some polyazamacrocyclic acetates containing pyridine,'' *Inorg. Chem.* **34**, 2233–2243 (1995).
36. D. S. Hubbard, S. Chang, M. P. Houlne, and D. J. Bornhop, ''Environmental effects on the luminescent properties of tissue-selective polyaazamacrocyclic pyridyl chelates of terbium,'' submitted to *Appl. Spectroscopy* (Feb. 1998).
37. D. J. Bornhop, D. S. Hubbard, M. P. Houlne, G. E. Kiefer, B. C. Pence, and D. L. Morgan, ''Enhanced imaging of rat colon cancer using a fluorescent tissue site-selective metal chelate marker, Tb-PTCMB,'' submitted to *Biophys. J.* (February 1998).
38. E. Soni and T. Lougren, ''Time resolved fluorescence of lanthanide probes and application in biotechnology,'' *CRC Crit. Rev. Anal. Chem.* **18**(2), 105–154 (1987).
39. C. M. Gardner, S. L. Jacques, and A. J. Welch, ''Light transport in tissue: accurate expressions for one-dimensional fluence rate and escape function based upon Monte Carlo simulation,'' *Lasers Surg. Med.* **18**, 129–138 (1996).
40. Personal communication with Steven L. Jacques, Laser Biology Research Laboratory, University of Texas, M. D. Anderson Cancer Center, Houston, TX.